
Article:
Barakali, B., Ford, K.L. orcid.org/0000-0002-1080-6193 and Khamas, S.K. (2018) A High Gain Pattern Reconfigurable Micro-strip Dipole Antenna with a Gain Enhancing Partially Reflecting Surface. IET Microwaves, Antennas and Propagation, 12 (10). pp. 1679-1683. ISSN 1751-8725

https://doi.org/10.1049/iet-map.2018.0150

IET Research Journals

A High Gain Pattern Reconfigurable Micro-strip Dipole Antenna with a Gain Enhancing Partially Reflecting Surface

The Institution of Engineering and Technology

A High Gain Pattern Reconfigurable Micro-strip Dipole Antenna with a Gain Enhancing Partially Reflecting Surface

ISSN 1751-8644
doi: 0000000000
www.ietdl.org

Beyit Barakali, Kenneth Lee Ford, Salam Khamas*

Department of Electronic and Electrical Engineering, University of Sheffield, Mappin Street, Sheffield, UK
** E-mail: l.ford@sheffield.ac.uk*

Abstract: A beam reconfigurable antenna with high gain is presented with low complexity switching capability. The design consists of a printed dipole antenna with reconfigurable parasitic elements that are combined with a partially reflecting surface (PRS) to provide main lobe radiation pattern switching between boresight and close to end-fire at an operating frequency of 1.81GHz. The reconfigurability is achieved using only two PIN diodes and the measured gain of the antenna is 8.5dBi gain at boresight and 14.3dBi towards the end-fire direction.

1 Introduction

In recent years, research into reconfigurable antennas has increased on account of being a potential candidate to overcome the latest challenges introduced with the current mobile networks as well as an infrastructure for the future communication systems. Some of the challenges are, but not limited to the limited frequency spectrum, inefficient high energy consuming systems as well as the complexity of the structures [1, 2]. Reconfigurable parameters of an antenna can be classified as the polarization, resonant frequency and pattern where a variety of examples of achieving such reconfigurations are presented in [3–8]. Reconfiguring the pattern of an antenna is proposed to improve or establish a communication link between various antennas at different directions or adjusting beams towards the intended users. A patten reconfigurable antenna is also beneficial in preventing electronic jamming and can be used to steer away from the congested traffic which in turn can improve the security[9, 10]. Conventional techniques involved in achieving pattern reconfiguration include mechanical tuning where physical parts of the structure are adjusted and also phased arrays which are bulky, high cost and complex structures limiting the use for many applications. Accordingly, the interest in low complexity and low cost antennas are of particular interest. Notable research in this area, [1, 9–11], develop the use of reconfigurable parasitic elements where the current paths on the parasitics are altered with the aid of diodes or photo-switching conductors. Using this approach the parasitic elements can be configured as reflectors or directors for low gain applications. A method of enhancing gain at boresight was introduced, [12], where partially reflecting surfaces (PRS) were adopted, and further developed, [13, 14], using single and multilayer partially reflecting surfaces to achieve gains of approximately 20dBi. Artificial magnetic conductors (AMC) have also been used in conjunction with partially reflecting surface as a superstrate where a gain of 19dBi is reported, [15]. Furthermore, in [16] a slot coupled patch is used for gain enhancement of a cavity type resonator showing a measured peak gain of 13.8dBi at boresight. Alternative methods of placing the radiating element between the ground plane and partially reflecting surface have been proposed, [17, 18], and up to 15dBi gain has been reported. Recently a study of generating high gain pattern reconfigurable antenna based on the partially reflecting surface model investigated in [12] is presented in [19] where unit-cells forming the partially reflecting surface structure are connected together with PIN diodes in order to generate a non uniform structure to control the beam direction where substantial amount of components are used and complex circuitry is needed to vary the biasing conditions. In this paper, a low complexity, high gain, beam reconfiguring antenna is proposed. Unlike previous work, with the aid of only two active components controlled over a single bias line, an antenna which can switch the main beam between boresight and endfire direction is presented. The paper develops the design process from Fabry-Perot theory through to the design of the partially reflecting surface and antenna which is then compared against measured results.

2 High Gain Beam Reconfigurable Concept and Design Methodology

The proposed reconfigurable antenna is illustrated in Fig. 1a as a cross section through the centre of the antenna. A radiating dipole antenna with two parasitics spaced on either side, Fig. 1b, is placed over a ground plane at a distance, h. The antenna radiation is controlled by the use of PIN diodes placed at the centre of the parasitic elements. A partially reflecting surface, Fig. 1c, is placed a distance, h_c, away from the ground plane in order to create a cavity and enhance the gain. In designing the antenna to achieve boresight and endfire radiation two methodologies were adopted. Firstly, when the PIN diodes are switched off the parasitic elements are non-resonant at the design frequency and have a minimal effect on the radiation pattern. In this case the spacing, h_c can be determined using Fabry-Perot analysis. Secondly, when the PIN diodes are switched on the parasitic elements are resonant and if spaced appropriately away from the fed dipole will enhance the gain towards the endfire direction. It has been assumed throughout that the design frequency is 1.8GHz to demonstrate the functionality but also is then applicable to typical communications networks.

2.1 Fabry-Perot Topology

The Fabry-Perot resonance condition, [12], can be adopted to calculate the required PRS spacing for enhancing the directivity towards the intended direction. Multiple reflections are generated within the cavity formed by the ground and PRS as shown in Fig. 1a. The phase difference between the direct and the first reflected wave can be determined with (1)

$$\Theta_1 = \frac{2\pi}{\lambda} 2\ell \tan\alpha \sin\alpha - \frac{2\pi}{\lambda}\frac{2\ell}{\cos\alpha} - \pi + \psi \qquad (1)$$

where λ is the freespace wavelength, l is the spacing between the PRS and ground plane, α is the angle of incidence, and ψ is the reflection phase of the PRS.

Previous studies [12, 14, 15, 20] revealed that, according to the phase differences introduced with distinctive path lengths within the

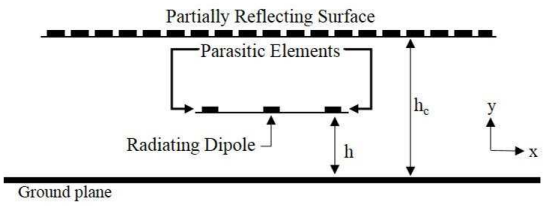

(a) Cross section

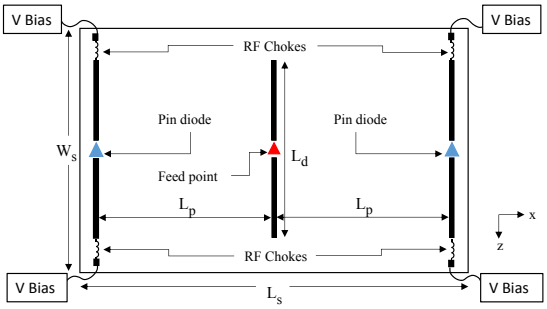

(b) Antenna design

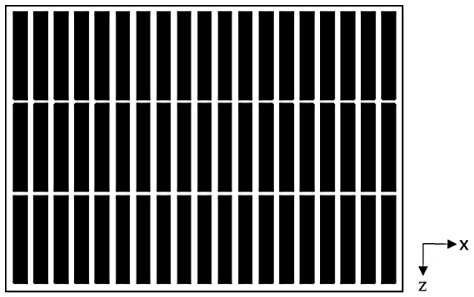

(c) PRS cross section

Fig. 1: Proposed model

cavity, the directivity at boresight can be determined, when $\alpha = 0^0$, as shown in (2-3);

$$D = \left(\frac{[1-\rho^2]}{1+\rho^2-2\rho cos(\phi)}\right) \tag{2}$$

where the phase difference between direct and the reflected wave is represented with $\phi = \psi - \phi_{GND} - \frac{4\pi}{\lambda}\ell\cos\alpha$ and ϕ_{GND} is the reflection phase of the ground plane. The resonant height for gain enhancement can be described using (3)

$$h_c = \frac{\lambda}{4\pi}(\psi + \phi_{GND} - 2N\pi) \qquad N = 0, 1, 2... \tag{3}$$

where N is an integer number. The spacing, h, between the antenna and ground plane can be determined using (4)

$$\phi_{GND} = \pi - 2\tan^{-1}\left(\frac{Z_d \tan\left(\frac{2\pi h}{\lambda}\right)}{Z_0}\right) \tag{4}$$

where Z_d and Z_0 are the characteristic impedances of the spacer material and freespace respectively.

2.2 *Partially Reflecting Structure and Unit-cell analysis*

The unit cell of the partially reflecting surface is illustrated in Fig. 2a which comprises of a metallic patch of thin copper with length L,

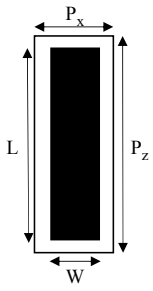

(a) unitcell

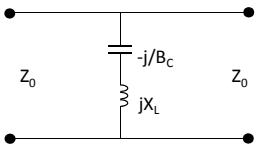

(b) Equivalent circuit of unit cell

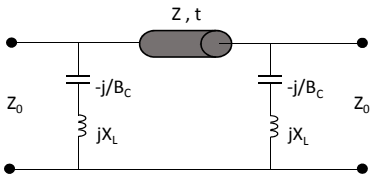

(c) Complete equivalent circuit

Fig. 2: Unit cell, equivalent circuit and complete model analysis

width W and the unit cell periodicity is P_x and P_z which is etched on a 0.8mm thick FR4 substrate ($\varepsilon_r = 4.3, tan\delta = 0.025$) and the equivalent circuit is shown in Fig. 2b. Equivalent circuit parameters are calculated using (5) and (6), [21],

$$X_L = \frac{KP_xZ_0\left(\frac{P_z - g_{zeff}}{P_z}\right)}{\lambda}\left[ln\left(cosec\left[\frac{\pi w_{eff}}{2P_x}\right]\right)\right] \tag{5}$$

$$B_C = \frac{4K_{eff}KP_z\left(\frac{w_{eff}}{P_x}\right)}{Z_0\lambda}\left[ln\left(\frac{2P_z}{\pi g_{zeff}}\right)\right] \tag{6}$$

where $w_{eff} = 1.68W\sqrt{\frac{P_x - W}{P_x}}$, $g_{zeff} = 0.29\sqrt[4]{P_z - L}\sqrt{\frac{P_z}{P_x}}$ and $K = \frac{P_z}{P_x\sqrt{L}}$. The remaining term, K_{eff}, can be estimated using (7).

$$K_{eff} = 0.475 f_1 f_2 f_3 \tag{7}$$

where

$$f_1 = 1 - 1.37\left(\frac{P_z - W}{P_z}\right)\left[\tanh\left(25\frac{P_z - W}{P_z}\right)\right]^2 \tag{8}$$

$$f_2 = 1 - \exp\left(-13t_s + \frac{13}{\epsilon_r}\sqrt{\frac{t_s}{\epsilon_r}}\right) \tag{9}$$

$$f_3 = \frac{\epsilon_r}{(\tanh\left[\sqrt{\epsilon_r}\right])^2} \tag{10}$$

and t_s and ϵ_r are the substrate thickness and relative permittivity respectively.

The overall equivalent circuit of the Fabry-Perot resonator is shown in Fig. 2c where the ground plane of the resonator is removed and image theory is employed by adding a second PRS a distance $t = 2h_c$ away, [22]. Maximising the transmission coefficient will then provide a Fabry-Perot resonance. Following this design approach the PRS dimensions are L=97.5mm, W=15.15mm, P_z=102mm and P_x=22.72mm for a resonance at 1.85GHz where the frequency was chosen both for demonstration purposes and is also a typical cellular transmission frequency. Full field simulations were carried out for comparison using CST microwave studio where the resonator was modelled as a unit cell of an infinite structure by adopting a Floquet mode analysis. The transmission coefficient of

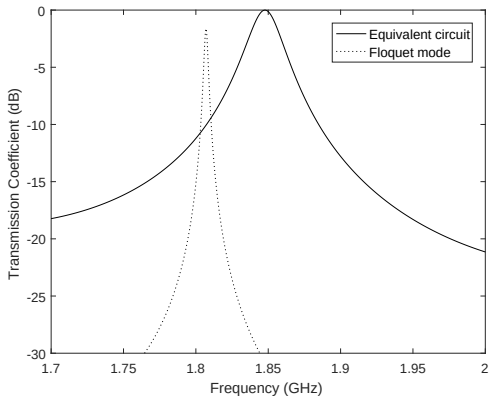

Fig. 3: Simulated equivalent circuit and floquet model for $h_c = \lambda$

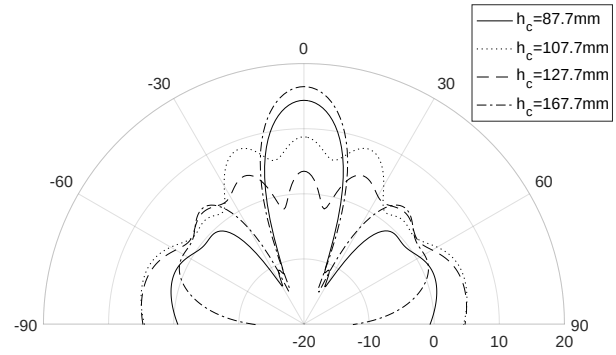

Fig. 5: Simulated realized H-plane gain patterns with "OFF" State PIN diodes at the resonant frequency of $1.8GHz$

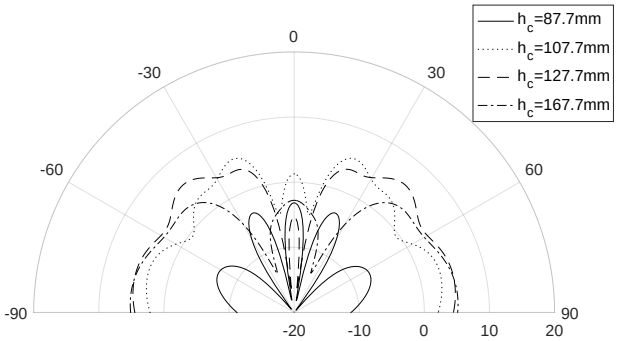

Fig. 4: Simulated realized H-plane gain patterns with "ON" State PIN diodes at the resonant frequency of $1.8GHz$

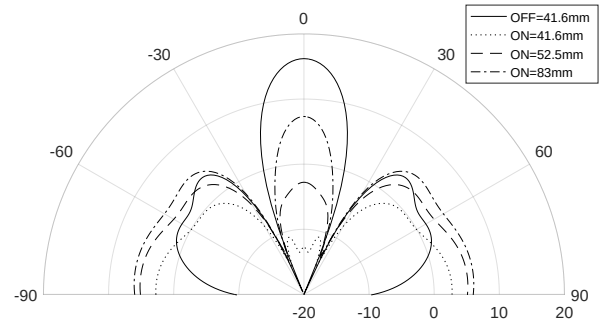

Fig. 6: Realized H-plane gain simulation results with variable parasitic element spacings with "ON" and "OFF" states PIN diodes for $h_c = \lambda$

both the equivalent circuit and full field simulation are shown in Fig. 3 when the spacing between the PRS and ground plane is a wavelength. The results show a slight shift in resonant frequency from 1.8GHz to 1.85GHz and a difference in bandwidth, however, for a proof of principle this was deemed sufficient.

2.3 Antenna Design and Full Structure Analysis

Fig. 1b illustrates a schematic representation of a dipole antenna with two parasitic elements on each side with equal lengths on a FR-4 substrate with a thickness of $1.6mm$ which is designed to operate at 1.8GHz. **This can be related to the well know Yagi-Uda antenna topology which is an endfire radiating antenna consisting a radiating element, reflector and directors. An increased length of a parasitic strip relative to the radiating element have an inductive behaviour which is used as a reflector and a shorter strip is capacitive directing the beam towards the intended direction [10].** At the proposed design the parasitic elements are chosen to be resonant in order to have maximum impact on the radiation pattern. The parasitic elements are placed a distance L_p either side of the radiating dipole and are formed of two thin metallic strips connected with PIN diodes as represented in Fig. 1b. For evaluation purposes a lumped component model of the Infineon Technologies BAR64-02V was used to enable comparisons with measurements. When the PIN diodes are forward biased the equivalent circuit is a series resistor(R_{PIN}) and inductor(L_{PIN}) with the values of $R_{PIN} = 1.35\Omega$ and $L_{PIN} = 0.6nH$. In the reverse bias state the equivalent circuit can be represented as a series RLC where the component values for the resistance, inductance and capacitance are $R_{PIN} = 1.35\Omega$, $L_{PIN} = 0.6nH$ and $C_{PIN} = 0.17pF$ respectively. RF choke inductors (22nH) are implemented to limit currents at the edge of parasitics. The antenna is placed a quarter wavelength above a ground plane,with dimensions of 550x$550mm$.

To simulate the complete high gain antenna the PRS is placed a distance h_c above the ground plane. For evaluation purposes the partially reflecting surface was formed using 19 by 3 unit cells, using the unit cell dimensions determined from section 2.2, that was found to be sufficiently large enough to provide maximum radiation. It is understood from Fabry-Perot analysis that there are a number of choices for h_c where the resonant conditions apply, however, a trade-off between borsight and endfire gain needs to be carried out for the "ON" and "OFF" diode states. The trade-off was carried out by varying h_c between $\lambda/2$ and λ. The simulated realized gain (H-plane) for the "ON" and "OFF" diode states are shown in Fig. 4 and Fig. 5. It can be seen from Fig. 4, for the "ON" state, that for a cavity spacing of $h_c = \lambda/2$ there is very poor radiation performance which is due to the impedance match of the antenna to the 50Ω source. In this case the simulated reflection coefficient magnitude was -2.2dB. As the cavity spacing is increased the endfire radiation improves with a good trade-off between high endfire and low boresight gain being achieved when $h_c = \lambda$ and the gain is 5dBi at endfire.

The results shown in Fig. 5, for the "OFF" state show high gain for both the $h_c = \lambda/2$ and $h_c = \lambda$ cavity spacing as expected from the Fabry-Perot analysis with a moderately higher gain (16.5dBi) when $h_c = \lambda$. For this case the reflection coefficient magnitude was -9.3dB. To combine the boresight and endfire requirements a cavity spacing of $h_c = \lambda$ is appropriate.

To determine an appropriate spacing, L_p, a number of simulations were carried out with the diodes in the forward bias state (ON) where the maximum radiation towards endfire is required. The simulated realized gain is shown in Fig. 6. For comparison the reverse bias state (OFF) is shown where it was found that the realized gain was independent of L_p. It can be seen from Fig. 6 that a good compromise between maximising endfire radiation whilst reducing boresight gain can be found when $L_p = 52.5mm$ which equates to approximately $\lambda/3$. A more detailed analysis of the previously optimised partially

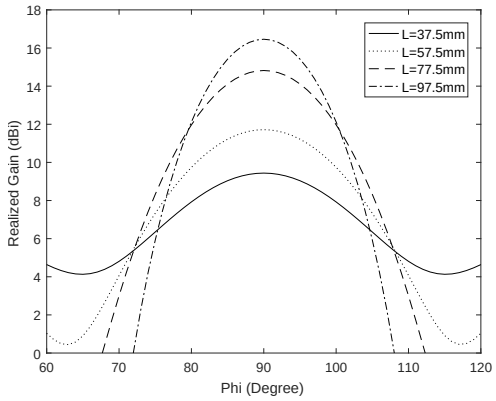

Fig. 7: Simulated realized H-plane gain of the complete model operating at $1.8GHz$ with varied patch lengths where cavity distance is $h_c = 167.7mm$

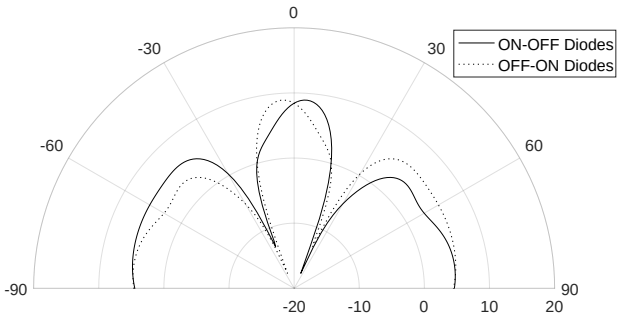

Fig. 8: Simulated realized H-plane gain patterns with "ON-OFF" and "OFF-ON" state PIN diodes at the resonant frequency of $1.8GHz$

reflecting surface patch length, $L = 97.5mm$, was carried out to determine if there was any impact on performance. The realized gain in the "OFF" state is shown in Fig. 7. This result shows that high gain is achieved which validates the original unit cell simulations.

Simulation results of "ON-OFF" and "OFF-ON" PIN diode states are evaluated for completeness and are presented in Fig. 8. It can be seen that in this mode a more balance radiation performance between boresight and endfire can be achieved with gains of 8dBi and 5dBi respectively. As might be expected the radiation patterns are asymmetric due to the bias conditions of the parasitic elements.

Simulated radiation and total efficiency are plotted against frequency in Fig. 9 where the "OFF" state realised gain is above 80% over the displayed frequency range and the losses are predominately due to the FR4 substrate, the total efficiency reduces to a minimum of 50% due to antenna mismatch. This mismatch is due to the presence of the PRS but could be alleviated with the use of an external matching circuit. When the switches are "ON" the radiation efficiency is 68% at 1.8GHz which is mainly due to PIN diode resistance and the total efficiency is 61% as antenna mismatch is reduced. The realised gain is shown in Fig. 10 and it can be observed that with "ON" state PIN diodes, the gain variation over a 100MHz frequency band is approximately 0.7db which can be accepted as reasonably stable and wideband compared to typical communication bandwidths. In the "OFF" state, there is increased gain variation, however, over a 20MHz bandwidth the variation is only 0.9dB which would be sufficient for many communication applications.

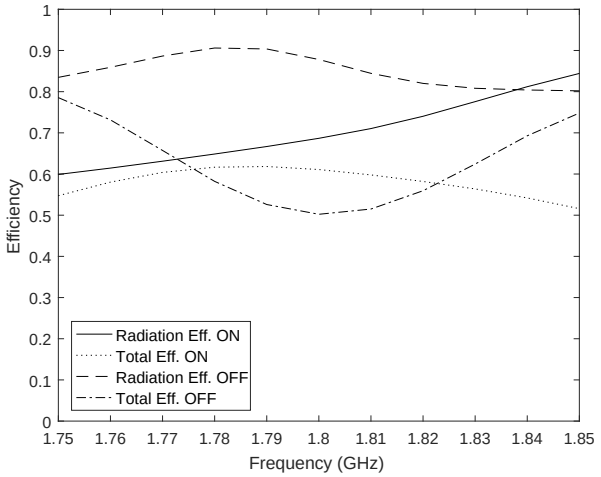

Fig. 9: Simulated total and radiation efficiency over frequency with "ON" and "OFF" state diodes

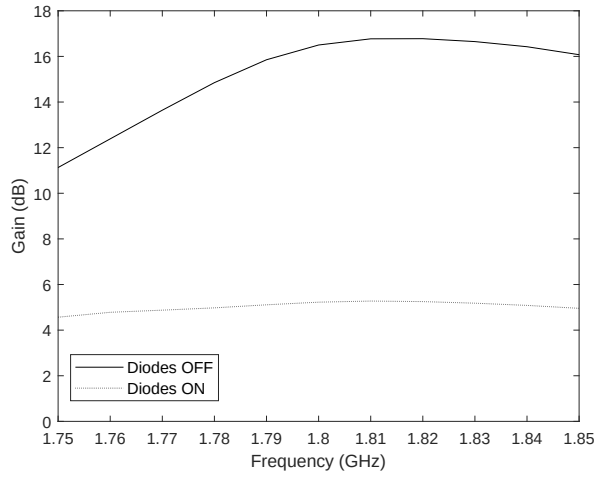

Fig. 10: Simulated gain over frequency with "ON" and "OFF" state diodes

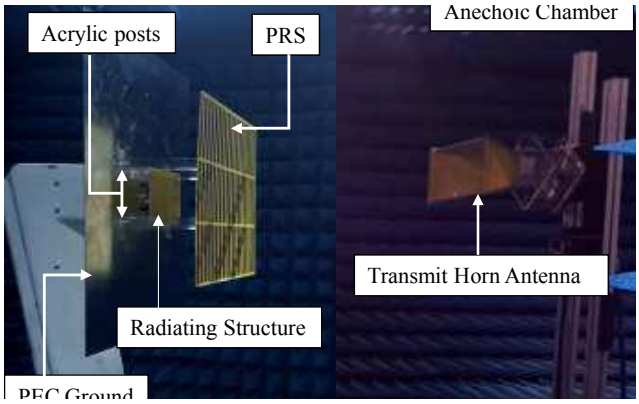

Fig. 11: Experimental configuration in the Anechoic Chamber

3 Experimental Results

A prototype antenna was manufactured using standard PCB etching techniques for both the partially reflecting surface and

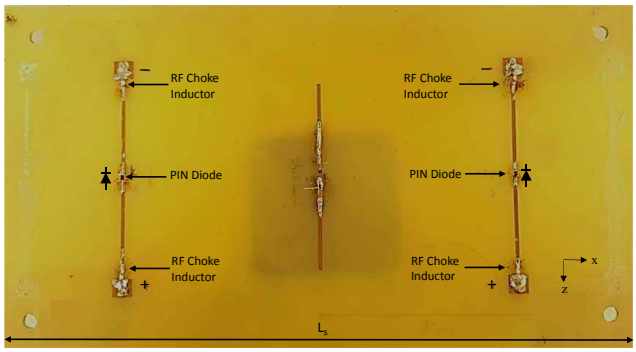

Fig. 12: A detailed capture of Radiating Dipole and Parasitics indicating the biasing points, PIN diodes and RF choke inductors

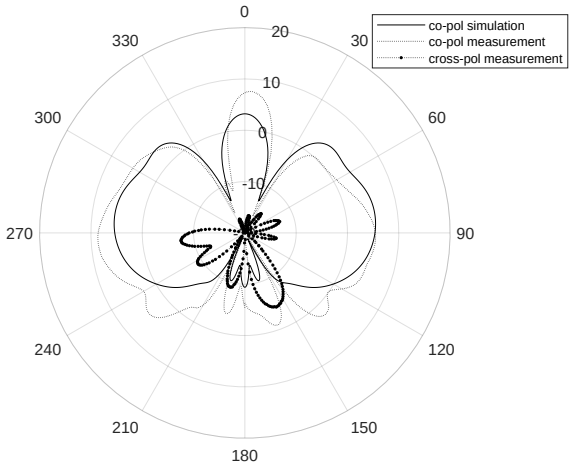

Fig. 13: Measured and simulated co and cross polarised ON state H-plane radiation pattern

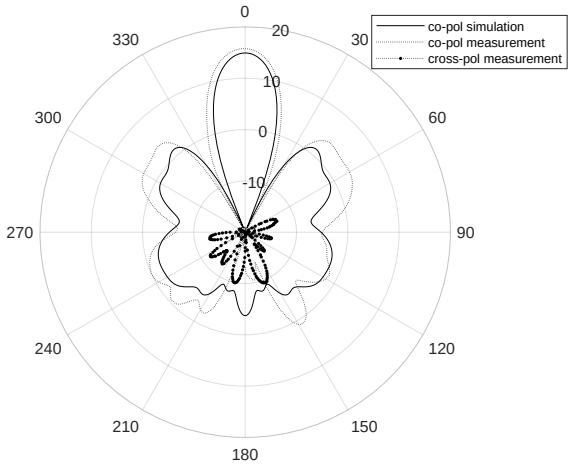

Fig. 14: Measured and simulated co and cross polarised OFF state H-plane radiation pattern

dipole/parasitic elements. The dipole was fed using a balanced semi-rigid coaxial cable with a quarter wave balun. Measurements were carried out at 1.8GHz in a fully anechoic chamber where a transmitting antenna (R&S® HF 906) was placed 2.5m away from the antenna under test (AUT). The AUT was mounted on a horizontally rotating arm where the complex S-parameters were measured using an Agilent Technologies E5071C ENA Series vector network analyser (VNA) over a range of angles between $\pm 180^\circ$ in 1° steps. The measurements were carried out automatically using the NSI 2000® system. The PIN diode control voltage was applied using a dc power supply placed outside the chamber in order to have minimum interference with the far-field response. Measurements were also carried out where the AUT was replaced with a R&S® HF 906 with known gain. The S21 measurements of the AUT and known antenna were then compared to infer the realized gain of the AUT. Fig. 11 and Fig. 12, show the photographs of experimental set-up within the chamber and a closer capture of the radiating dipole with parasitics where the components and biasing points are clearly identified. Simulations of the manufactured AUT were carried out for comparison. The simulated and measured realized gains for co and cross polarizations with ON and OFF state PIN diodes are shown in Fig. 13 and Fig. 14. Evaluating the results achieved in Fig. 13 and Fig. 14, a considerable difference between ON and OFF states of the PIN diodes can be observed. At boresight a there is a maximum gain of 15.8 dBi for the OFF diode state as compared to a gain of 7.3dBi in the ON state. Similarly analysing the behaviour of radiation pattern towards end-fire (270°), the gain switches between -6.5dBi and 8.6dBi for the OFF and ON diode states respectively. It can be seen that there is an asymmetry in the pattern giving an OFF/ON gain at 90° of -5.0dBi/5.5dBi. The measured reflection coefficient magnitude was -18.3dB and -5.5dB for the ON and OFF diode states respectively. Correspondingly the simulation results are in a good agreement with measurement results, Fig. 13, show endfire switching between -6.9dBi to 5.59dBi and Fig. 14, boresight gains of 14.9 dBi and 3.2 dBi.

4 Conclusion

In this paper a low complexity high gain beam switching antenna has been proposed and is capable of boresight and end-fire operation. The approach details how two PIN diodes embedded within parasitic resonant elements can be used to reconfigure the radiation pattern and when combined with a partially reflecting surface produces an increase in gain. Full field simulation results have been compared against experimental measurements and show similar trends for a 1.8GHz operating frequency. The results show that the gain can be switched at boresight by $8.5dBi$ whilst a $15.1dBi$ change in gain is observed at end fire. Future work will focus on further enhancement of gain for dual polarized applications.

5 Acknowledgements

Authors are thankful to the EPSRC (Engineering and Physical Sciences Research Council) for funding this project.

6 References

1 Y. Y. Bai, S. Xiao, C. Liu, X. Shuai, and B. Z. Wang, "Design of pattern reconfigurable antennas based on a two - Element dipole array model," *IEEE Transactions on Antennas and Propagation*, vol. 61, no. 9, pp. 4867–4871, 2013.

2 J. Ren, X. Yang, J. Yin, and Y. Yin, "A Novel Antenna with Reconfigurable Patterns Using H-Shaped Structures," *IEEE Antennas and Wireless Propagation Letters*, vol. 14, no. 1, pp. 915–918, 2015.

3 J. T. Bernhard, *Reconfigurable Antennas*, vol. 2. Morgan & Claypool Publishers, 2007.

4 S. Genovesi, A. D. Candia, and A. Monorchio, "Compact and low profile frequency agile antenna for multistandard wireless communication systems," *IEEE Transactions on Antennas and Propagation*, vol. 62, no. 3, pp. 1019–1026, 2014.

5 J. Kiriazi, H. Ghali, H. Ragaie, and H. Haddara, "Reconfigurable dual-band dipole antenna on silicon using series MEMS switches," *IEEE Antennas and Propagation Society International Symposium. Digest. Held in conjunction with: USNC/CNC/URSI North American Radio Sci. Meeting (Cat. No.03CH37450)*, vol. 1, pp. 403–406, 2003.

6 C. J. Panagamuwa, A. Chauraya, and J. C. Vardaxoglou, "Frequency and beam reconfigurable antenna using photoconducting switches," *IEEE Transactions on Antennas and Propagation*, vol. 54, no. 2, pp. 449–454, 2006.

7 A. Khidre, K.-f. Lee, F. Yang, and A. Z. Elsherbeni, "Circular Polarization Recon fi gurable Wideband E-Shaped Patch Antenna for Wireless Applications," *Ieee Transactions on Antennas and Propagation*, vol. 61, no. 2, pp. 260–263, 2013.

8 M. A. Kossel, S. Member, K. Roland, and H. Benedickter, "An Active Tagging System Using Circular-Polarization Modulation," *IEEE TRANSACTIONS ON MICROWAVE THEORY AND TECHNIQUES*, vol. 47, no. 12, pp. 2242–2248, 1999.
9 X. S. Yang, B. Z. Wang, W. Wu, and S. Xiao, "Yagi patch antenna with dual-band and pattern reconfigurable characteristics," *IEEE Antennas and Wireless Propagation Letters*, vol. 6, pp. 168–171, 2007.
10 S. Zhang, G. H. Huff, J. Feng, and J. T. Bernhard, "A pattern reconfigurable microstrip parasitic array," *IEEE Transactions on Antennas and Propagation*, vol. 52, no. 10, pp. 2773–2776, 2004.
11 C. J. Panagamuwa, A. Chauraya, and J. C. Vardaxoglou, "Frequency and beam reconfigurable antenna using photoconducting switches," *IEEE Transactions on Antennas and Propagation*, vol. 54, no. 2, pp. 449–454, 2006.
12 G. Trentini, "Partially reflecting sheet arrays," *IRE Transactions on Antennas and Propagation*, vol. 4, no. 4, pp. 666–671, 1956.
13 K. Konstantinidis, A. P. Feresidis, and P. S. Hall, "Multilayer partially reflective surfaces for broadband fabry-perot cavity antennas," *IEEE Transactions on Antennas and Propagation*, vol. 62, no. 7, pp. 3474–3481, 2014.
14 A. Feresidis and J. Vardaxoglou, "High gain planar antenna using optimised partially reflective surfaces," *IEE Proceedings - Microwaves, Antennas and Propagation*, vol. 148, no. 6, p. 345, 2001.
15 A. P. Feresidis, G. Goussetis, S. Wang, and J. C. Vardaxoglou, "Artificial magnetic conductor surfaces and their application to low-profile high-gain planar antennas," *IEEE Transactions on Antennas and Propagation*, vol. 53, no. 1 I, pp. 209–215, 2005.
16 N. Wang, Q. Liu, C. Wu, L. Talbi, Q. Zeng, and J. Xu, "Wideband fabry perot resonator antenna with two complementary FSS Layers," *IEEE Transactions on Antennas and Propagation*, vol. 62, no. 5, pp. 2463–2471, 2014.
17 N. Wang, J. Li, G. Wei, L. Talbi, Q. Zeng, and J. Xu, "Wideband Fabry Perot Resonator Antenna With Two Layers of Dielectric Superstrates," *in IEEE Antennas and Wireless Propagation Letters*, vol. 14, pp. 229–232, 2015.
18 Z. M. Razi, P. Rezaei, and A. Valizade, "A novel design of Fabry-Perot antenna using metamaterial superstrate for gain and bandwidth enhancement," *AEUE - International Journal of Electronics and Communications*, vol. 69, no. 10, pp. 1525–1532, 2015.
19 L. Y. Ji, Y. J. Guo, P. Y. Qin, S. X. Gong, and R. Mittra, "A reconfigurable partially reflective surface (PRS) antenna for beam steering," *IEEE Transactions on Antennas and Propagation*, vol. 63, no. 6, pp. 2387–2395, 2015.
20 Z.-g. Liu, "Fabry-Perot Resonator Antenna," *Journal of Infrared, Millimeter, and Terahertz Waves*, no. November 2008, pp. 391–403, 2009.
21 S. B. Savia and E. A. Parker, "Equivalent circuit model for superdense linear dipole fss," *IEE Proceedings - Microwaves, Antennas and Propagation*, vol. 150, pp. 37–42, Feb 2003.
22 K. R. Jha and G. Singh, "Design of highly directive cavity type terahertz antenna for wireless communication," *OPTICS*, vol. 284, no. 20, pp. 4996–5002, 2011.